SCIENCE CHINA
Earth Sciences

• RESEARCH PAPER •

April 2015 Vol.58 No.4: 604–614
doi: 10.1007/s11430-014-4989-y

Comparisons of GCM cloud cover parameterizations with cloud-resolving model explicit simulations

WANG XiaoCong*, LIU YiMin, BAO Qing & WU GuoXiong

State Key Laboratory of Numerical Modeling for Atmospheric Sciences and Geophysical Fluid Dynamics, Institute of Atmospheric Physics, Chinese Academy of Sciences, Beijing 100029, China

Received June 16, 2014; accepted September 2, 2014; published online January 5, 2015

Three kinds of the widely-used cloudiness parameterizations are compared with data produced from the cloud-resolving model (CRM) simulations of the tropical cloud system. The investigated schemes include those based on relative humidity (RH), the semi-empirical scheme using cloud condensate as a predictor, and the statistical scheme based on probability distribution functions (PDFs). Results show that all three schemes are successful in reproducing the timing of cloud generation, except for the RH-based scheme, in which low-level clouds are artificially simulated during cloudless days. In contrast, the low-level clouds are well simulated in the semi-empirical and PDF-based statistical schemes, both of which are close to the CRM explicit simulations. In addition to the Gaussian PDF, two alternative PDFs are also explored to investigate the impact of different PDFs on cloud parameterizations. All the PDF-based parameterizations are found to be inaccurate for high cloud simulations, in either the magnitude or the structure. The primary reason is that the investigated PDFs are symmetrically assumed, yet the skewness factors in deep convective cloud regimes are highly significant, indicating the symmetrical assumption is not well satisfied in those regimes. Results imply the need to seek a skewed PDF in statistical schemes so that it can yield better performance in high cloud simulations.

cloud cover, relative humidity, statistical cloud scheme, PDFs, CRM, KWAJEX

Citation: Wang X C, Liu Y M, Bao Q, et al. 2015. Comparisons of GCM cloud cover parameterizations with cloud-resolving model explicit simulations. Science China: Earth Sciences, 58: 604−614, doi: 10.1007/s11430-014-4989-y

Uncertainties of cloud simulations in climate modeling are one of the principal obstacles preventing accurate prediction of climate change (Webster and Stephens, 1984). Numerous studies have shown that model simulations are sensitive to the specification of cloudiness (Meleshko and Wetherald, 1981; Shukla and Sud, 1981; Zhang et al., 2013). In the last two decades, growing attentions have been paid to the cloud parameterization (Lohmann et al., 1999; Bogenschutz and Krueger, 2013). Although significant progresses have been made and most cloud schemes at present are state-of-the-art, it is widely recognized that uncertainties in cloud parameterizations remain the major cause of discrepancies between observations and simulations. Though a thorny issue it is, the importance of cloud parameterization can never be overemphasized, as clouds have an important impact on atmospheric circulations and climate via regulating Earth's radiation budget (Wang and Zhao, 1994).

Among all the difficulties arising in cloud parameterizations, the following two are the most important. One comes from the cloud cover parameterization, which is essentially subject to the subgrid-scale nature of cloud-related processes (Randall et al., 2007). The other arises from cloud microphysical processes in dealing with cloud particles and hydrometeors. The above two are the so-called cloud macrophysics and microphysics. Traditionally, cloud fractions

*Corresponding author (email: wangxc@lasg.iap.ac.cn)

are parameterized empirically using relative humidity (RH) as a predictor; while cloud condensation processes are represented by cloud microphysical schemes, in which various processes such as condensation (evaporation), deposition (sublimation) and coagulation are explicitly treated. Since a few artificial assumptions are used in deriving the cloud parameterization, both cloud macrophysics and microphysics are confronted with great uncertainties. Moreover, the two aspects always interact with each other, causing the problem more complex, as on one hand the cloud cover acts as an input for cloud microphysical schemes to get local cloud properties, on the other hand the cloud microphysics typically alter the cloud cover. Such a problem must be addressed if one wants to adapt an explicit cloud microphysics scheme into host models with coarse resolution (Chosson et al., 2014).

Since most of the cloud microphysical schemes employed in large-scale models are of comparable complexity to those used in cloud-resolving models, the improvement on cloud cover parameterization is getting more and more urgent. The "all-or-nothing" approach was addressed by assuming no subgrid-scale fluctuations within a host grid (Ose, 1993; Fowler et al., 1996). Although such an assumption holds well for high-resolution models, it is inappropriate to apply it in large-scale models where turbulent- and convective-scale processes are usually unresolved. Fractional cloud parameterizations are thus proposed, which are empirically related with the grid-scale RH and the critical RH (Sundqvist, 1978; Slingo, 1980). The latter is introduced in an attempt to account for subgrid-scale variability. To better represent stratocumulus, other factors such as vertical velocity, and static stability are replenished in later development. Distinguished from the RH-based empirical schemes, the Probability Distribution Function (PDF) based statistical schemes own their inherent advantages in treating subgrid-scale variability, as subgrid-scale fluctuations can be readily obtained given the PDFs. The pioneer work of such schemes dates back to Sommeria and Deardorff (1977), Mellor (1977), and Bougeault (1981), in which the Gaussian PDF is adopted. The challenge of these schemes lies in the specification of an appropriate PDF for the saturation deficit S, as well as the determination of its moments such as variance and skewness. Various PDFs have been proposed in the literature and most of them are symmetrically assumed (Chen, 1991; Bechtold et al., 1995). The more complicated PDF like beta function, which takes skewness into account, is aimed for cirrus parameterization (Tompkins, 2002). To avoid the difficulty to specify the PDF and its moments, Cuijpers and Bechtold (1995) proposed a simple parameterization, which is essentially based on a unimodal distribution computed as a linear combination of a Gaussian distribution (for stratiform clouds) and an exponential distribution (for cumulus clouds). In this scheme, no further knowledge about the distribution function or the moments is needed. Due to its simplicity, the scheme is employed in the spectral atmospheric model developed at the State Key Laboratory of Numerical Modeling for Atmospheric Physics and Geophysical Fluid Dynamics, Institute of Atmospheric Physics (LASG/IAP) (Dai et al., 2005).

In between the RH-based empirical and PDF-based statistical schemes are semi-empirical schemes. The canonical one is proposed by Xu and Randall (1996a), which related cloud cover to RH and cloud hydrometeors. Although the PDFs are not explicitly used, the scheme can be viewed as manifestations of a statistical scheme where the actual PDF is not given, but the time-mean statistics of its integral are (Tompkins, 2002).

The above three kinds of cloud cover parameterizations as well as their variants are widely used in large-scale models. However, fewer studies were documented regarding their performances (Xu and Randall, 1996b). Previous studies suffered from either scarcities of cloud observational dataset or non-linear interactions between dynamical and physical components. In this study, the cloud-resolving model is used to surmount these difficulties, since the CRM simulations can not only server as good surrogates, but also provide abundant subgrid-scale information which is usually unavailable in regular observations. It is also accessible to validate the PDFs in the literature in statistical cloudiness parameterizations.

1 CRM case description and simulations

1.1 Case description

The field experimental campaign chosen in this study is the Tropical Rainfall Measuring Mission (TRMM) Kwajalein Experiment (KWAJEX), which occurred in Marshall Islands (7°–10°N, 166°–169°E) with frequent convections. This case has been widely used and described in previous studies (Schumacher et al., 2008; Wang and Zhang, 2013). Figure 1 displays the observed temperature, moisture and their vertical advective tendencies, which are derived from the constrained variational analysis (Zhang and Lin, 1997; Zhang et al., 2001). Strong dynamic cooling in middle and upper troposphere (Figure 1(c)) along with the pronounced moisture convergence in lower levels (Figure 1(d)) is noted, which is in favor of deep convection.

1.2 Model and experiments

The cloud-resolving model used in this study is a three-dimensional, time-dependent model named SAM, which was kindly provided by Marat Khairoutdinov of Stony Brook University. The dynamical framework of the model is based on the anelastic equations of motion. The prognostic thermodynamical variables of the model are liquid water/ice moist static energy, total nonprecipitating water, and total precipitating water. The model has been widely used in convection and cloud studies (Fan et al., 2009; Oreopoulos

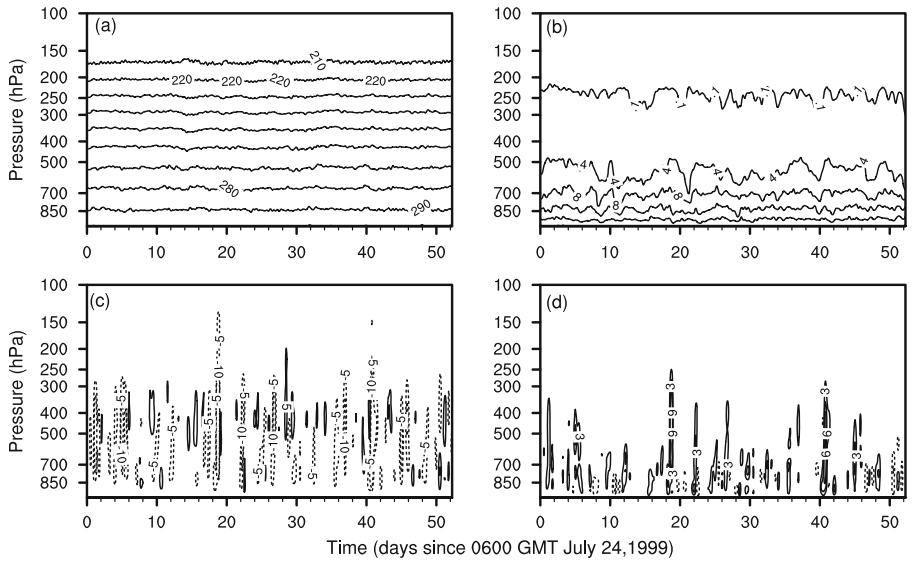

Figure 1 Observations for TRMM KWAJEX. (a) Temperature (K); (b) specific humidity (g kg^{-1}); vertical advection of (c) temperature (K d^{-1}) and (d) moisture (g kg^{-1} d^{-1}). In (c) and (d), contour interval is 5 and 2, respectively. Solid lines are for contours greater than or equal to zero and dotted lines for contours less than zero.

and Khairoutdinov, 2003; Wang and Zhang, 2014). More detailed information about SAM is referred to Khairoutdinov and Randall (2003).

The CRM run uses initial soundings and time-dependent forcings based on the constrained optimization method of Zhang et al. (2001) for the time period of 24 July–14 September 1999. The simulation uses 64 vertical levels with grid spacing that increase smoothly from 75 m at the surface to a nearly uniform spacing of 400 m through the troposphere and a larger spacing of 1 km in the Newtonian damping region between 19 km and model top (27 km). A horizontal grid of 256×256 points is used with a resolution of 1 km.

1.3 Model simulations

Figure 2(a) and (b) presents the simulated temperature T, specific humidity Q as well as their biases against observations. Although intermittent moist biases exist near the middle level, the model generally well reproduces the observed temperature and moisture, with the error within the range of ±5 K for T and ±1.5 g kg^{-1} for Q. Flaky cold biases in high levels are likely due to errors in the observational datasets. The simulated surface precipitation is shown in Figure 2(c), associated with the observed rainfall. As expected, the simulation exhibits remarkably similar and realistic behavior in either the occurrence or the magnitude of the precipitation. Figure 2(d) gives the shaded cloud fraction (optical depth>0.3) (black), top-of-atmosphere (TOA) outgoing longwave radiation OLR (blue) and daily averaged TOA reflected shortwave radiation (RSR) (red). In a comparison between Figure 2(c) and (d), it is noted that heavy precipitation is usually associated with an increase in cloud fraction, thereby corresponding to a decrease of OLR and an increase of RSR, implying a parallel relation between precipitation and outgoing longwave (reflected shortwave) radiation.

The outstanding performance of SAM guarantees us to use its simulation as a substitution for observations, from which both grid and subgrid thermodynamic variables can be obtained. To further ease the analysis, a fragment of two days is extracted from the whole integration period, during which a strong precipitation event is covered. For the extracted fragment, the simulations of precipitation, relative humidity (RH), cloud fraction, cloud water/ice and rain/snow are displayed in Figure 3. The perfect simulation of precipitation is again noticed (Figure 3(a)). From the view of microscopies, the heavy rainfall is attributed to the large mass of rain/snow in upper levels, which falls to the ground with a significant terminal velocity (Figure 3(e)). The center of cloud water/ice is above the frozen level (Figure 3(d)), indicating cold cloud precipitating process predominates. Strong precipitation is closely related with high RH in middle levels and large cloud fraction in upper levels (Figure 3(b), (c)). In calculating RH, the algorithm for saturation specific humidity is distinguished between water and ice, depending on temperature. If $T \geqslant 0$°C, the saturation specific humidity is assumed to be with respect to water; otherwise, it is with respect to ice. Although it is clear that RH plays an important role in parameterizing cloud cover, it is undoubtedly that RH is not a perfect predictor.

2 Cloud cover algorithms in the literature

Prior to the performance comparisons of cloud cover parameterizations, a brief description of the general methodology of their mathematic formulations is given. Three cloud cover parameterizations are presented, including the

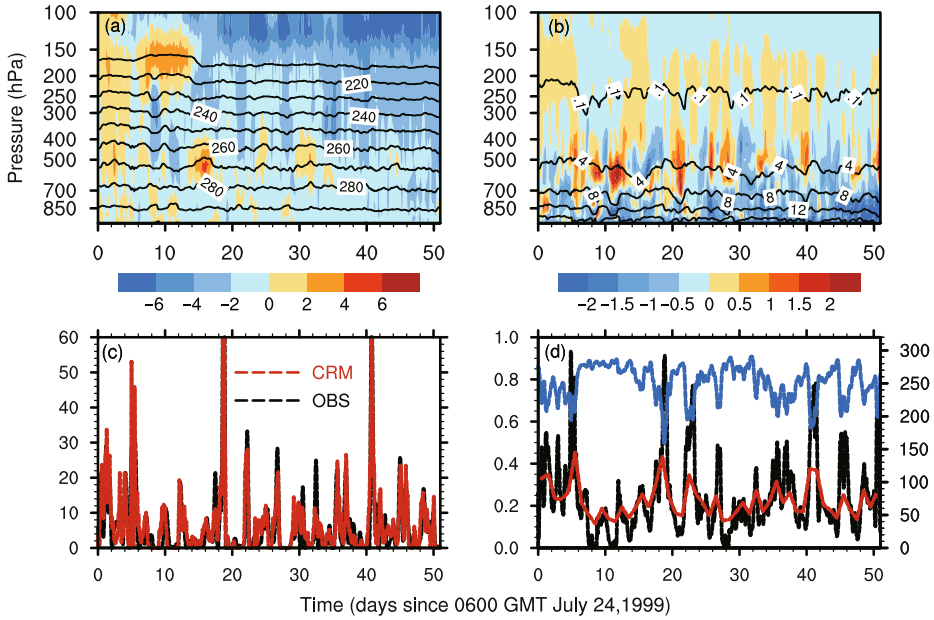

Figure 2 CRM simulations for TRMM KWAJEX. (a) Temperature (K); (b) specific humidity (g kg^{-1}); (c) precipitation (mm d^{-1}); (d) shaded cloud fraction (black), OLR (blue) and daily averaged TOA reflected shortwave radiation (red) (W m^{-2}). Differences between simulations and observations are shaded in (a) and (b).

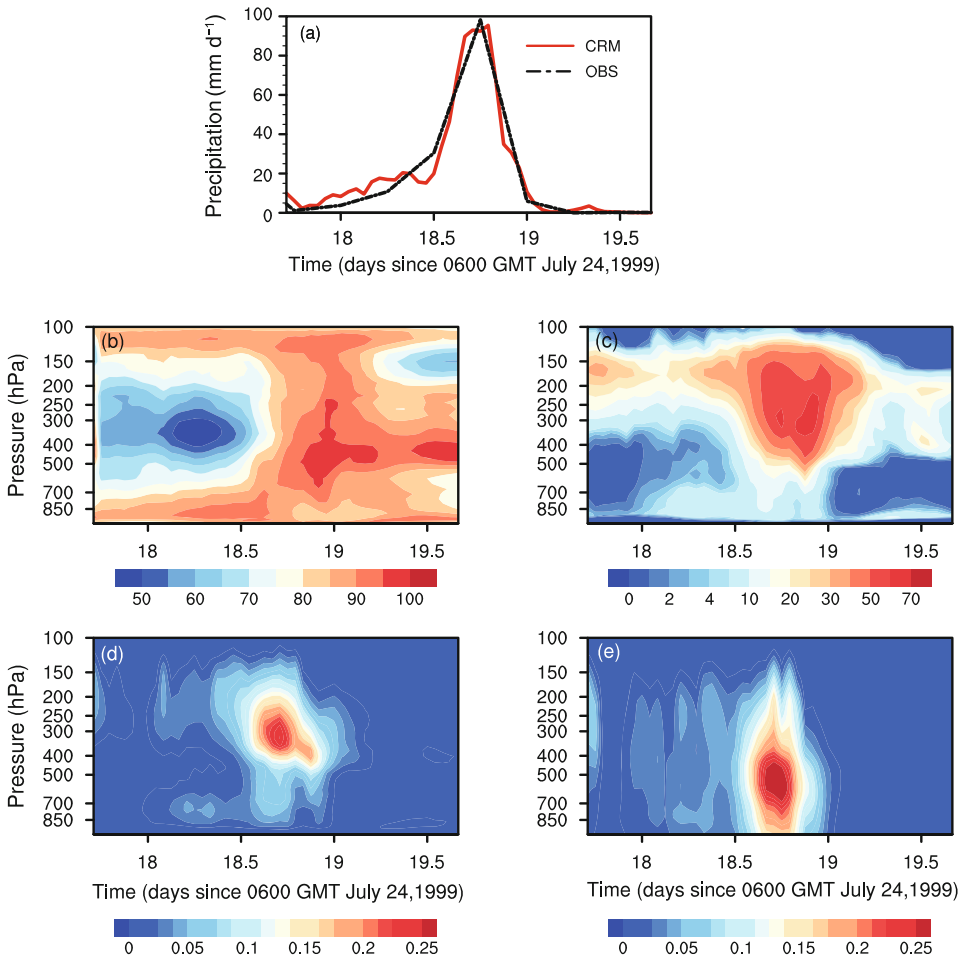

Figure 3 CRM simulations for TRMM KWAJEX. (a) Precipitation; (b) relative humidity (%); (c) cloud fraction (%); (d) cloud water/ice (g kg^{-1}); (e) rain/snow (g kg^{-1}).

RH-based empirical scheme, the semi-empirical scheme and the PDF-based statistical scheme.

2.1 RH-based empirical scheme

For this kind of scheme, fractional cloud cover C is an empirical function of RH written as eq. (1), where r is the grid-mean RH and r_o is a condensation threshold specified as a function of height following Xu and Krueger (1991), which is expressed in eq. (2). The threshold r_o is assumed to decrease with height, implying condensation is easier to occur in upper levels than in lower levels under the same r. Growth of existing clouds or formation of new clouds occurs if $r > r_o$. Conversely, an existing cloud is dissipated by evaporation or sublimation once $r > r_o$.

$$C = 1 - \sqrt{1 - \frac{r - r_o}{1 - r_o}}, \tag{1}$$

$$r_o = 0.7 + 0.2\exp\left[1 - \left(\frac{p_s}{p}\right)^4\right]. \tag{2}$$

2.2 Semi-empirical scheme

The semi-empirical cloudiness parameterization addressed by Xu and Randall (1996a) uses the large-scale average condensate (cloud water/ice) as the primary predictor, in addition to the grid-mean RH. The formulation is expressed as

$$C = r^p\left[1 - \exp(-\alpha\overline{q}_l)\right], \tag{3}$$

where p and α are tunable parameters equaling 0.25 and 100, respectively. As implied in eq. (3), C will gradually approach its upper limit r^p as $\overline{q}_l$ increases. On the contrary, once $\overline{q}_l$ equals 0, no cloud exists regardless of RH.

2.3 PDF-based statistical scheme

Sommeria and Deardorff pioneered statistical scheme on the basis of bivariate normal function of two conserved thermodynamic variables: total water q_t and liquid potential temperature θ_l. Since water vapor perturbations can be correlated with temperature perturbations, which alter the local saturation vapor pressure, the joint PDF between q_t and θ_l thus can be reformulated in terms of a single variable s, defined as the saturation deficit

$$s = a_l(q_t' - \alpha_l\theta'), \tag{4}$$

where the primes denote the derivation from the mean state, and the constants are defined as

$$\alpha = \partial q^*(\overline{\theta}_l)/\partial\overline{\theta}_l, \tag{5}$$

$$a_l = \left[1 + L/c_p\partial q^*(\overline{\theta}_l)/\partial\overline{T}_l\right]^{-1}. \tag{6}$$

The overbar in eqs. (5) and (6) stands for the grid-mean state, q^* is the saturation water vapor mixing ratio, and T_l is the liquid water temperature. Physically, s describes the distance between the thermodynamic state and the linearized saturation vapor mixing ratio curve. The departure of the mean state from saturation is expressed as

$$\Omega_0 = a_l(\overline{q}_t - q^*(\theta_l))/\sigma_s. \tag{7}$$

Thus the cloud fraction C, and the cloud condensate $\overline{q}_l$ are determined by

$$C = \int_{-\Omega_0}^{+\infty} P(s)\mathrm{d}s, \tag{8}$$

$$\overline{q}_l = \int_{-\Omega_0}^{+\infty} (s + \Omega_0)P(s)\mathrm{d}s, \tag{9}$$

where $P(s)$ is the PDF of s. Given a Gaussian distribution, the analytical solution of cloud fraction C and cloud condensate $\overline{q}_l$ can be readily obtained, expressed as

$$C = \frac{1}{2}\left[1 + erf\left(\frac{\Omega_0}{\sqrt{2}\sigma_s}\right)\right], \tag{10}$$

$$\overline{q}_l = \Omega_0 C + \frac{\sigma_s}{\sqrt{2\pi}}\exp\left[-\frac{1}{2}\left(\frac{\Omega_0}{\sigma_s}\right)^2\right], \tag{11}$$

where $erf(x)$ is the error function

$$erf(x) = \frac{2}{\sqrt{\pi}}\int_0^x \exp(-u^2)\mathrm{d}u. \tag{12}$$

The stand deviation of $s(\sigma_s)$ is derived according to eq. (4), written as

$$\sigma_s = a_l\sqrt{q_t'^2 - 2\alpha_l\theta_l'q_t' + \alpha_l^2\theta_l'^2}, \tag{13}$$

which is a combination of the variance of θ_l (σ_{θ_l}) and q_t(σ_{q_t}), as well as their covariance. The above equations are widely used in previous studies (Tompkins, 2002; Xu and Randall, 1996b). In most cases, σ_{θ_l} and σ_{q_t} predominate over their covariance, which are presented in Figure 4. Large variances are observed during the strong convective period, demonstrating that subgrid-scale turbulences in those days are rather intense.

3 Performance comparisons of various cloudiness parameterizations

3.1 Comparisons of parameterized cloud cover

Figure 5 gives the cloud amounts that were calculated with the above three schemes, as well as the original CRM explicit simulation. Overall, all three parameterizations are successful in reproducing the locations of the maxima cloud

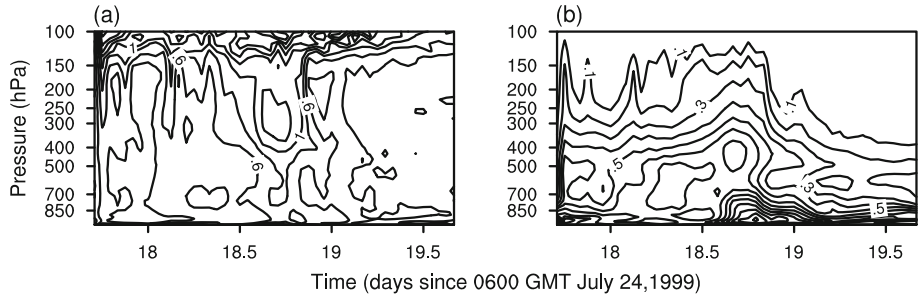

Figure 4 Stand deviations for liquid water potential temperature (K) (a) and total water (g kg^{-1}) (b).

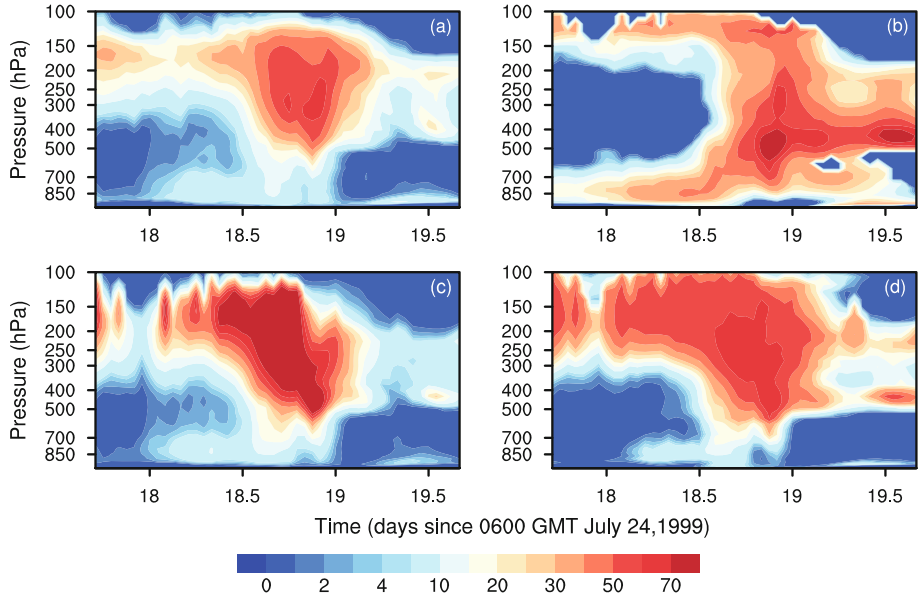

Figure 5 Cloud cover simulated by CRM (a), RH-based empirical scheme (b), semi-empirical scheme (c), and Gaussian PDF-based statistical scheme (d) (%).

amount between day 18.5 and day 19. However, the magnitudes are somewhat over predicted, especially for the semi-empirical scheme. For statistical schemes, the over-prediction of middle and high cloud is due partly to the poor assumption that supersaturation is not allowed to occur during the condensation process. Although it is a good approximation for warm clouds, it is not for ice clouds, as observations have shown large supersaturations with respect to ice often exist (Tompkins, 2002). Relaxing the assumption by taking supersaturation into account is beyond the scope of this study, and will be the subject of future research. Although the RH-based empirical scheme well simulates the time location of maxima cloud, it fails in reproducing the vertical structure, as the altitude of cloud center is systematically lower compared with CRM simulations. Furthermore, low clouds after day 19 are artificially produced. The poor performance is understandable, as the scheme is heavily dependent on RH though the condensation threshold r_o is introduced. Increasing r_o leads to a decrease in cloud fraction C, whereas decreasing the value of r_o causes an increase in C. Thus for this case, r_o in low and middle levels is significantly underestimated. Although we can adjust r_o to get a perfect cloud structure in this case, it can hardly be universal. In reality, r_o has a large variation in space and altitude (Quaas, 2012). The Gaussian PDF-based statistical scheme performs much better, especially for the low cloud. Note the low level cloudlessness after day 19 is also well reproduced. The semi-empirical scheme shows a comparable performance with the PDF-based scheme, and even better in the low cloud simulation. Although RH is still a predictor in the semi-empirical scheme, the scheme is more dependent on the other predictor: cloud condensate $\overline{q}_l$. For example, if $\overline{q}_l$ equals 0, there will be no cloud no matter how large RH is. In fact, such dependence is clearly reflected in Figure 3, as the pattern of cloud water/ice resembles cloud structure more than that of RH.

3.2 Impacts of different PDFs on cloud parameterization

In addition to the Gaussian PDF discussed above, two other widely-used PDFs are also explored to investigate the im-

pact of different PDFs on cloud parameterizations. A sharp PDF based on triangular distribution function and a smooth PDF based on broad distribution function are employed (Smith, 1990; Lohmann et al., 1999), which are defined as eqs. (14) and (15), respectively.

$$P(s)=\begin{cases}0, & s\leqslant-\sqrt{6},\\ \frac{1}{6}(\sqrt{6}-|s|), & -\sqrt{6}<s<\sqrt{6},\\ 1, & s\geqslant\sqrt{6},\end{cases} \tag{14}$$

$$P(s)=\frac{4}{\pi(4+s^4)}. \tag{15}$$

Visual examination of the two alternative PDFs as well as the Gaussian PDF is given in Figure 6(a). Given Ω_0 varying from –4 to 4, integrals of the r.h.s of eq. (8) with the specified $P(s)$ yield the corresponding cloud fraction C, which are shown in Figure 6(b).

The simulated cloud cover by two alternative PDFs are shown in Figure 7, along with those by the Gaussian PDF and the CRM simulation. Generally, the performances are much similar to that by Gaussian PDF, although tiny differences appear in low levels. This is because the three PDFs are much similar in the distribution (Figure 6(a)). Thus, their integrations with respect to the same lower limit (Ω_0) are also similar (Figure 6(b)). One noticeable difference lies in the region where $|\Omega_0|>1.5$. As displayed in Figure 6(b), the cloud fraction C calculated by the broad PDF is larger than those by the other two, which is attributed to larger weights within relatively dry regions. Given that the atmosphere is usually far away from saturation at low levels, the above analysis answers why the broad PDF produces more cloud than the other two in the lower troposphere.

In addition to cloud amount, the PDF-based statistical scheme can produce cloud condensate as well. In this sense, the cloud macrophysics and microphysics are treated in a consistent manner, as the cloud macrophysical and microphysical properties are obtained via the same PDF. The predicted cloud condensates according to eq. (9) are shown in Figure 8. Overall, all three schemes are successful in reproducing the cloud condensate center, although the magnitude is somewhat overestimated. The over- prediction of cloud hydrometeors arises from the non-precipitating assumption.

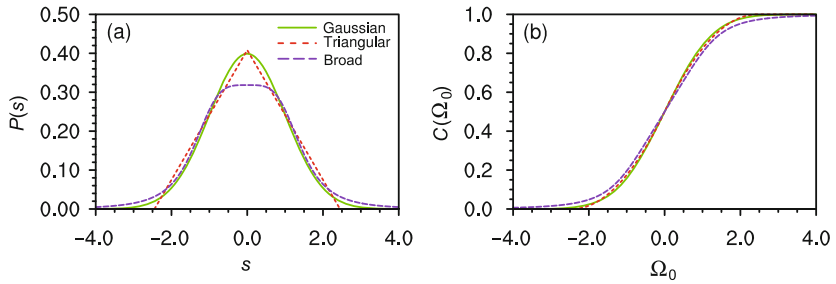

Figure 6 Probability distribution functions (a) and their integrations with respect to the lower limit Ω_0 (b).

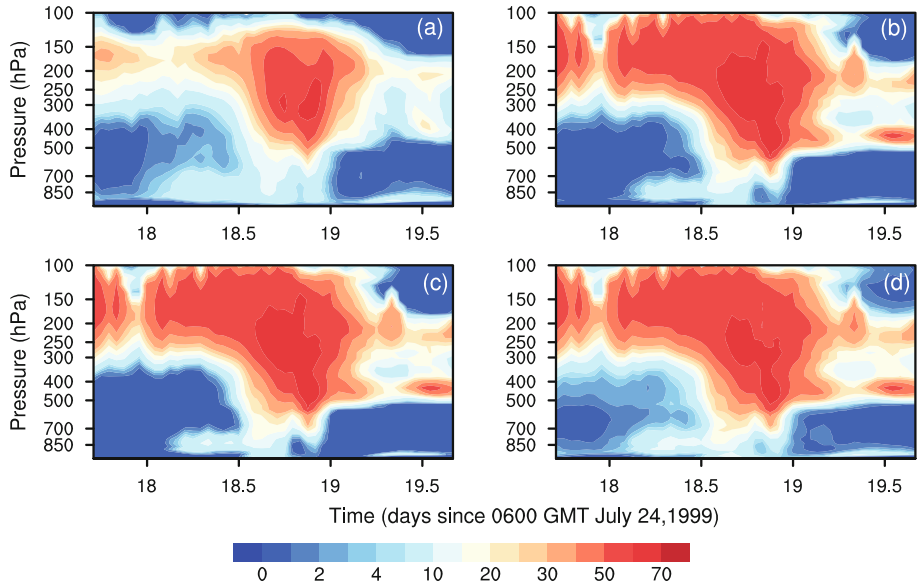

Figure 7 Cloudiness simulated by (a) CRM, (b) Gaussian PDF-based statistical scheme, (c) triangular PDF-based statistical scheme, and (d) broad PDF-based statistical scheme (%).

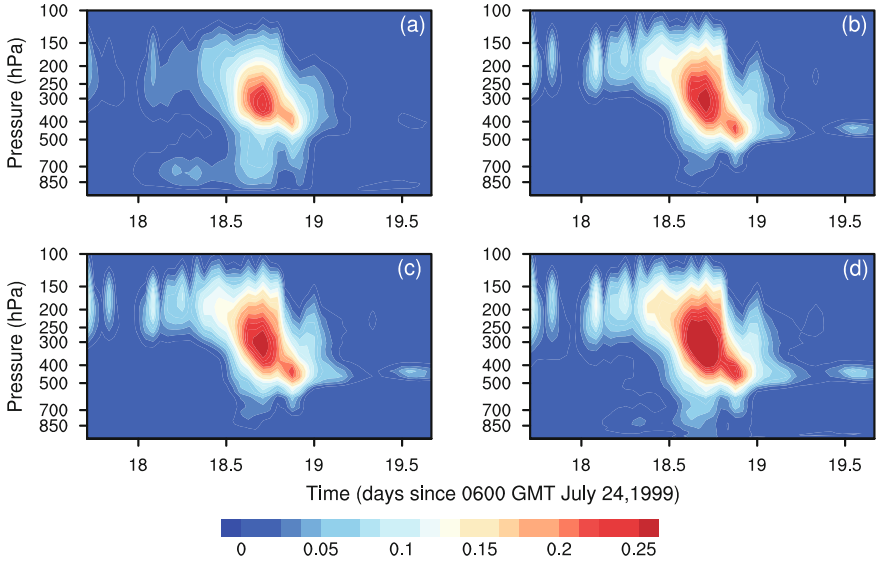

Figure 8 Cloud condensate simulated by (a) CRM, (b) Gaussian PDF-based statistical scheme, (c) triangular PDF-based statistical scheme, and (d) broad PDF-based statistical scheme (g kg^{-1}).

In fact, precipitating hydrometeors like rain/snow can be as large as cloud water/ice in strong convective events (Figure 3(e)). In consistency with the better performance in low cloud simulation with the broad PDF, the cloud condensate in low levels is also better simulated.

3.3 Problems of the symmetrical PDF

In essence, the symmetrical PDF-based statistical schemes depend on two variables, the departure of the mean state to saturation q_t–q_{sl} and the stand deviation of s(σ_s), which are shown in Figure 9(a) and (b). Widespread unsaturation is observed in low levels, while saturation occurs in upper levels during the strong precipitation period. The stand deviation σ_s generally decreases with height above 500 hPa, where the maximum σ_s is located. The pattern of σ_s shows a similar behavior to that of σ_{q_t} (Figure 4(b)). This is because fluctuations of temperature are likely to be smaller in magnitude than that of total water, especially in the tropics where gravity waves remove lateral fluctuations of temperature on fast timescales (Bretherton and Smolarkiewicz, 1989). The ratio of q_t–q_{sl} and σ_s, defined as the normalized departure to saturation (Ω_0), is presented in Figure 9(d). The pattern is extremely close to that of cloud cover C, as the latter is monotonously regulated by Ω_0 (Figure 6(b)).

While non-supersaturation assumption may partly account for cloudiness biases in high levels, it is not the culprit. The primary cause lies in the symmetrically assumed PDF. In fact, positive skewness is often observed during the convective process (Larson et al., 2001). Figure 9(c) gives

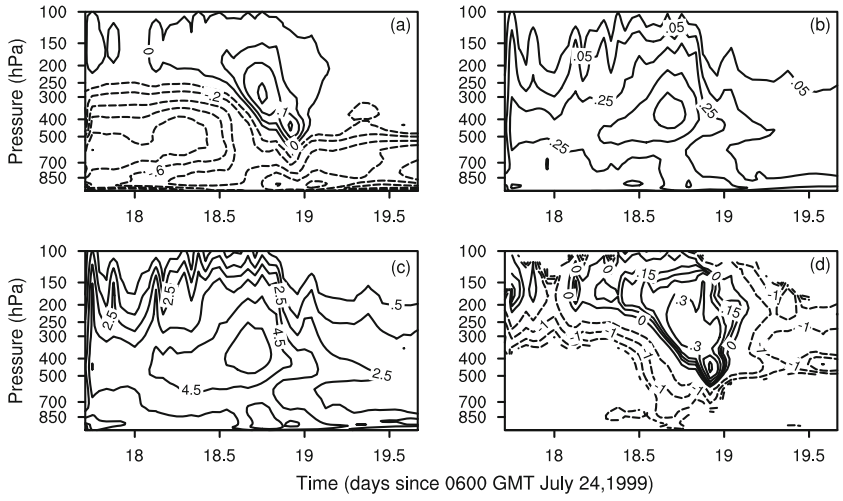

Figure 9 Time-pressure distribution for q_t–q_{sl} (g kg^{-1}) (a), stand deviation of S (μg kg^{-1}) (b), the third moment of S (g^3 kg^{-3}) (c), and normalized departure of the mean state from saturation (d).

the third moment of $s(\mu_s)$. As noticed, positive μ_s is widely spread, indicating S is not symmetrically distributed, but positively skewed.

To better illustrate this, Figure 10 gives the PDF of S at various model levels throughout the troposphere for one particular snapshot. The data are 65536 grid points in total for each level, and are divided into 200 bins of equal width. At lower heights, the distribution is approximately bell-shaped, and appears to be approximately unimodal, which well obeys the Gaussian distribution. However, at middle and upper heights, bimodal skewed distributions are observed instead, which is far away from the Gaussian distribution.

4 Discussion and conclusions

In this study, three kinds of the widely used cloudiness parameterizations have been evaluated with data produced from the CRM explicit simulations of tropical cloud systems during KWAJEX. With regard to the predicted cloud cover, the RH-based empirical scheme performs the worst among all of the three schemes, while the semi-empirical and PDF-based statistical schemes show a comparable performance. For the low cloud prediction, the semi-empirical scheme is even better than the PDF-based statistical scheme. However, it is important to point out here that there are essentially no clear distinctions among the three parameterizations. The only difference lies in the different treatment of subgrid-scale cloud-related processes. The RH-based scheme uses r_o in an attempt to account for the subgrid variability. If a time-invariant variance is used in a statistical scheme, it can be readily reduced to an RH-based scheme. Semi-empirical parameterizations such as Xu and Randall, which relate cloud fraction to both RH and cloud condensate, can be viewed as manifestations of a statistical scheme where the actual PDF is not known, but the grid-mean statistics of its integral are.

In addition to the Gaussian PDF, two alternative PDFs are also explored to investigate the impact of different PDFs on cloudiness parameterizations. Overall, their performances are much similar to that by Gaussian PDF. The underepprediction of low cloud in Gaussian and Triangular PDF is significantly improved in the broad PDF, which is due to

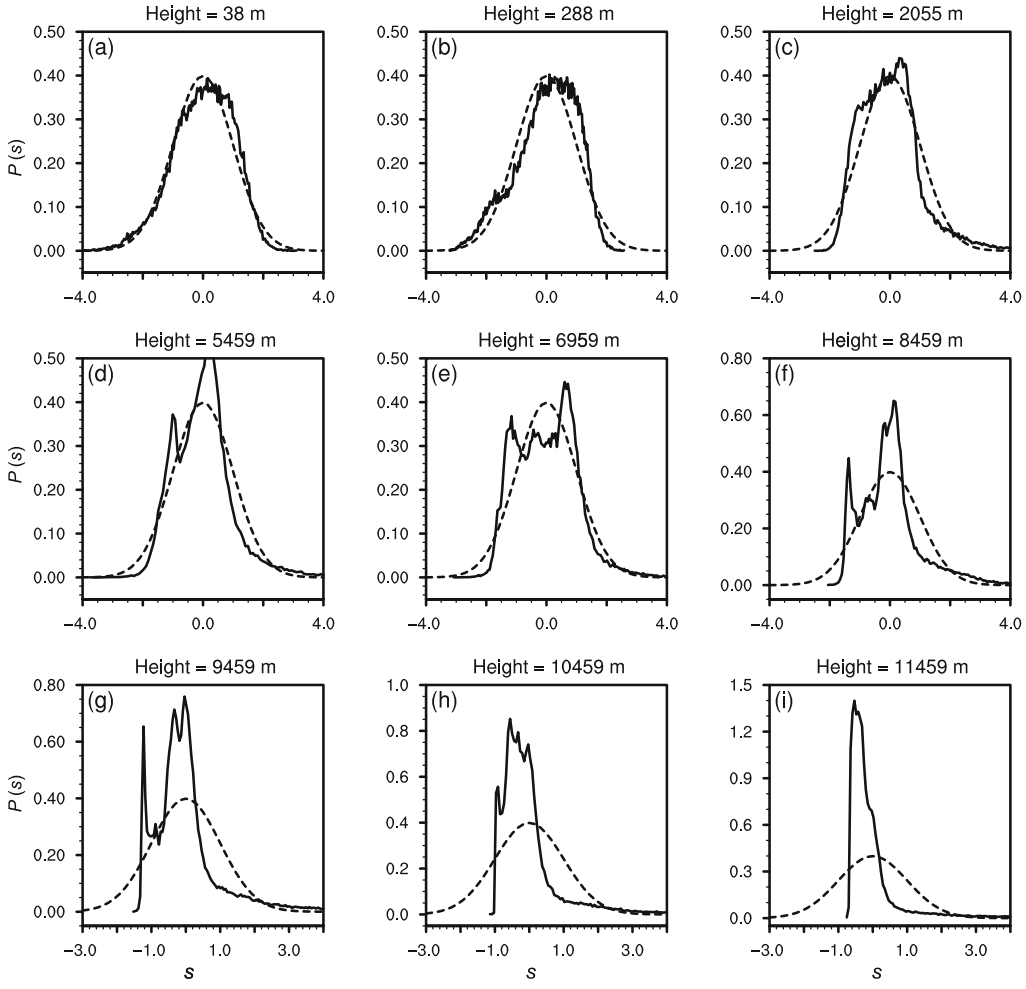

Figure 10 PDFs of S taken at various model levels at one snapshot (solid), with the Gaussian PDF as a reference (dashed).

larger weights within relatively dry regions. However, high cloud simulation is not getting better with the varied PDFs, which is essentially due to the symmetrical PDF assumption, which is positively skewed in reality. In fact, PDF-based parameterizations were originally intended for use in cloud-resolving models where subgrid cloudiness is only associated with turbulence-scale motion (Sommeria and Deardorff, 1997; Mellor, 1997), which can be appropriately deemed as symmetrically distributed. However, in large- scales models, a wide range of scales of motion, from turbulence through convection scale to mesoscale, coexist within a grid cell. Thus, high-order moments like skewness must be considered for convective cloud regimes, where the detrainment from deep convective updraft usually leads to a positive skewness of *S*. Tompkins (2002) took skewness into account with the aid of beta function, which can give both negatively skewed and positively skewed functions as well as symmetric Gaussian-like bell-shaped curves. The framework is outstanding, and sheds light on high cloud cover parameterizations in convective regimes. However, it is physically too complex. The determination of two shape parameters p and q in Tompkins's scheme remains unclear, although he provided approaches to relate the distribution moments to each physical process. Recently, Perraud et al. (2011) revisited the possibility of using most of the different distributions posed in the literature for a statistical description of Planet Boundary Layer (PBL) clouds. They found that shallow convections rooted in PBL typically lead to positively skewed distributions with a long flat tail in moist regions. Unimodal PDFs are found to be insufficient to correctly fit the long tail distributions. In contrast, bimodal distributions like the double Gaussian distribution allow a more accurate representation of the long tail, thus improving the simulations to some extent. While a bimodal distribution may be accurate enough to account for stratocumulus and stratus, it may not for cumulonimbus, particularly for the anvils caused by penetrative convections. In practice, it is most challenging to provide a unified approach for all cloud types. During the last two decades, encouraging progresses have been made in PBL cloud parameterizations, which constituted a hierarchy of schemes ranging from the independent cloud parameterizations to turbulence-convection-cloud coupled schemes (Akira et al., 2010; Lappen and Randall, 2001; Larson et al., 2002). For latter schemes, expensive computation cost is usually a burden, as higher order equations must be solved to close the system. It is therefore a trade-off between complexity and efficiency. Due to the poor understanding of deep convection, how to well represent the cirrus remains unclear. Although more complex joint PDFs may be helpful, it is desirable to seek simple assumed PDFs that can physically represent the skewness.

We thank the anonymous reviewers for their comments improving the original paper. This research was supported by the National Basic Research Program of China (Grant Nos. 2014CB441202, 2013CB955803), the National Natural Science Foundation of China (Grant Nos. 41305102, 91337110), the Strategic Priority Research Program of the Chinese Academy of Sciences (Grant No. XDA11010402), and the Joint Center for Global Change Studies (Grant No. 105019). This work was inspired during a longtime visit of the first author to SUNY at Stony Brook, for which he acknowledges financial support.

Akira K Y, Enomoto T, Ohfuchi W. 2010. An improved PDF cloud scheme for climate simulations. Q J R Meteorol Soc, 136: 1583–1597

Bechtold P, Cuijpers J, Mascart P, et al. 1995. Modeling of trade wind cumuli with a low-order turbulence model: Toward a unified description of Cu and Sc clouds in meteorological models. J Atmos Sci, 52: 455–463

Bogenschutz P A, Krueger S K. 2013. A simplified PDF parameterization of subgrid-scale clouds and turbulence for cloud-resolving models. J Adv Model Earth Syst, 5: 1–17

Bougeault P. 1981. Modeling the trade-wind cumulus boundary layer. Part I: Testing the ensemble cloud relations against numerical data. J Atmos Sci, 38: 2414–2428

Bretherton C S, Smolarkiewicz P K. 1989. Gravity waves, compensating subsidence and detrainment around cumulus clouds. J Atmos Sci, 46: 740–759

Chen J M. 1991. Turbulence-scale condensation parameterization. J Atmos Sci, 48: 1510–1512

Chosson F, Vaillancourt P, Milbrandt J, et al. 2014. Adapting two-moment microphysics schemes across model resolutions: Subgrid cloud and precipitation fraction and microphysical sub-time step. J Atmos Sci, 71: 2635–2653

Cuijpers J, Bechtold P. 1995. A simple parameterization of cloud water related variables for use in boundary layer models. J Atmos Sci, 52: 2486–2490

Dai F S, Yu R C, Zhang X H, et al. 2005. A statistically-based low-level cloud scheme and its tentative application in a general circulation model. Acta Meteorol Sin, 19: 263–274

Fan J, Yuan T, Comstock J M, et al. 2009. Dominant role by vertical wind shear in regulating aerosol effects on deep convective clouds. J Geophys Res,114: 1–9

Fowler L D, Randall D A, Rutledge S A. 1996. Liquid and ice cloud microphysics in the CSU general circulation model. Part I: Model description and simulated cloud microphysical processes. J Clim, 9: 489–529

Khairoutdinov M F, Randall D A. 2003. Cloud resolving modeling of the ARM summer 1997 IOP: Model formulation, results, uncertainties, and sensitivities. J Atmos Sci, 60: 607–625

Lappen C L, Randall D A. 2001. Toward a unified parameterization of the boundary layer and moist convection. Part I: A new type of mass-flux model. J Atmos Sci, 58: 2021–2036

Larson V E, Golaz J C, Cotton W R. 2002. Small-scale and mesoscale variability in cloudy boundary layers: Joint probability density functions. J Atmos Sci, 59: 3519–3539

Larson V E, Wood R, Field P R, et al. 2001. Small-scale and mesoscale variability of scalars in cloudy boundary layers: One dimensional probability density functions. J Atmos Sci, 58: 1978–1994

Lohmann U, McFarlane N, Levkov L, et al. 1999. Comparing different cloud schemes of a single column model by using mesoscale forcing and nudging technique. J Clim, 12: 438–461

Meleshko V P, Wetherald R T. 1981. The effect of a geographical cloud distribution on climate: A numerical experiment with an atmosphere general circulation model. J Geophys Res, 86: 11995–12014

Mellor G L. 1977. Gaussian cloud model relations. J Atmos Sci, 34: 356–358

Oreopoulos L, Khairoutdinov M. 2003. Overlap properties of clouds generated by a cloud-resolving model. J Geophy Res, 108: 1–15

Ose T. 1993. An examination of the effects of explicit cloud water in the UCLA GCM. J Meteorol Soc Jpn, 71: 93–109

Perraud, Couvreux, Malardel, et al. 2011. Evaluation of statistical distributions for the parameterization of subgrid boundary-layer clouds. Boundlayer Meteorol, 140: 263–294

Quaas J. 2012. Evaluating the "critical relative humidity" as a measure of subgrid-scale variability of humidity in general circulation model cloud cover parameterizations using satellite data. J Geophys Res, 117: 1–10

Randall D A, Wood R A, Bony S, et al. 2007. Climate models and their evaluation, in Climate Change: The physical science basis. Contribution of Working Group I to the Fourth Assessment Report of the Intergovernmental Panel on Climate Change. Cambridge: Cambridge University Press

Schumacher C, Ciesielski P E, Zhang M. 2008. Tropical cloud heating profiles: Analysis from KWAJEX. Mon Weather Rev, 136: 4289–4300

Shukla J, Sud Y. 1981. Effect of cloud radiation feedback on the climate of a general circulation model. J Atmos Sci, 38: 2337–2353

Slingo J M. 1980. A cloud parameterization scheme derived from GATE data for use with a numerical-model. Q J R Meteorol Soc, 106: 747–770

Smith R N. 1990. A scheme for predicting layer clouds and their water content in a general circulation model. Q J R Meteorol Soc, 116: 435–460

Sommeria, Deardorff J W. 1977. Subgrid-scale condensation in models of nonprecipitating clouds. J Atmos Sci, 34: 344–355

Sundqvist H. 1978. A parameterization scheme for non-convective condensation including prediction of cloud water content. Q J R Meteorol Soc, 104: 677–690

Tompkins A M. 2002. A prognostic parameterization for the subgrid-scale variability of water vapor and clouds in large-scale models and its use to diagnose cloud cover. J Atmos Sci, 59: 1917–1942

Wang H Q, Zhao G X. 1994. Cloud and radiation. Sci Atmos Sin, 18(Suppl): 910–932

Wang X C, Zhang M. 2013. An analysis of parameterization interactions and sensitivity of single-column model simulations to convection schemes in CAM4 and CAM5. J Geophys Res, 118: 1–12

Wang X C, Zhang M. 2014. Vertical velocity in shallow convection for different plume types. J Adv Model Earth Syst, 6: 478–489

Webster P J, Stephens G L. 1984. Cloud-radiation feedback and the climate problem. In: Houghton J T, ed. The Global Climate. Cambridge: Cambridge University Press

Xu K M, Krueger. 1991. Evaluation of cloudiness parameterizations using a cumulus ensemble model. Mon Weather Rev,119: 342–367

Xu K M, Randall D A. 1996a. A semi-empirical cloudiness parameterization for use in climate models. J Atmos Sci, 53: 3084–3102

Xu K M, Randall D A. 1996b. Evaluation of statistically based cloudiness parameterizations used in climate models. J Atmos Sci, 53: 3103–3119

Zhang H, Peng J, Jing X W, et al. 2013. The features of cloud overlapping in Eastern Asia and their effect on cloud radiative forcing. Sci China Earth Sci, 56: 737–747

Zhang M, Lin J. 1997. Constrained variational analysis of sounding data based on column-integrated budgets of mass, heat, moisture, and momentum: Approach and application to ARM measurements. J Atmos Sci, 54: 1503–1524

Zhang M, Lin J, Cederwall R, et al. 2001. Objective analysis of ARM IOP data: Method and sensitivity. Mon Weather Rev, 129: 295–311